



Excitonic contributions to dark matter-electron scattering

Downloaded from: <https://research.chalmers.se>, 2026-05-16 14:46 UTC

Citation for the original published paper (version of record):

Taufertshöfer, N., Zema, V., Catena, R. et al (2026). Excitonic contributions to dark matter-electron scattering. *Physical Review Research*, 8(1). <http://dx.doi.org/10.1103/9b1j-fcvw>

N.B. When citing this work, cite the original published paper.

Excitonic contributions to dark matter-electron scattering

Nora Taufertshöfer^{1,*}, Vanessa Zema^{2,3}, Riccardo Catena⁴, Valerio Olevano⁵ and Nicola A. Spaldin¹¹Materials Theory, ETH Zürich, 8093 Zurich, Switzerland²Max Planck Institute for Physics, 85748 Garching, Germany³Institut für Hochenergiephysik der Österreichischen Akademie der Wissenschaften, 1010 Wien, Austria⁴Chalmers University of Technology, Department of Physics, SE-412 96 Göteborg, Sweden⁵CNRS & Université de Grenoble Alpes, Institut Néel, 38042 Grenoble, France

(Received 5 August 2025; accepted 10 December 2025; published 20 January 2026)

We determine whether excitonic effects affect predictions of dark matter (DM)-electron scattering rates by calculating the energy- and momentum-dependent energy-loss function, including electron-hole interaction excitonic effects, for the DM scintillating detector materials GaAs and NaI. By comparing our results using the Bethe-Salpeter equation in the framework of many-body perturbation theory, which explicitly includes excitonic effects, with those using the quasiparticle random-phase approximation, which includes only electron-electron interaction and crystal local-field effects, we find that excitonic effects in NaI significantly increase the predicted scattering rate at low energy and as a result improve the cross-section sensitivity considering a realistic background. In contrast, the predicted scattering rate and the DM-electron scattering cross section for GaAs are minimally affected by excitonic effects.

DOI: [10.1103/9b1j-fcvw](https://doi.org/10.1103/9b1j-fcvw)

I. INTRODUCTION

Despite decades of direct detection efforts [1,2], the dark matter (DM) particle has yet to be observed. Until recently, experiments have primarily focused on searching for DM-induced nuclear recoils in low-background detectors, a strategy sensitive only to DM masses above about 1 GeV due to kinematic constraints. The absence of detection events in this mass range has prompted growing interest in sub-GeV DM, which would evade detection via nuclear recoil but could be detectable by its scattering with electrons [3–5]. Semiconducting targets, for example, in which the scattering process induces electron-hole excitation across the \sim eV band gap, allow sensitivity to DM particles with masses down to $\mathcal{O}(100)$ keV.

The first numerical predictions of DM-electron scattering rates in semiconducting crystals were made using electronic initial and final states derived from density functional theory (DFT) for silicon and germanium [6]. Many studies followed, comparing different target materials [7,8] and improving or extending the calculations [9–11], all within the DFT formalism. Importantly, it was established that the DM problem is separable from the calculation of the electronic structure [12,13], and that, for leading DM models that couple the DM

to the electron density, the DM-electron scattering rate can be written in terms of the dielectric function of the material and its related energy-loss function (ELF) [14,15]. These observations mean that the sophisticated machinery developed in the context of theoretical spectroscopy, such as the treatment of in-medium screening effects, collective excitations, and excitonic contributions using first-principles many-body perturbation theory (MBPT) beyond DFT, can be exploited in the calculation of DM-electron scattering rates. Previous works have considered the random phase approximation (RPA) [16] on top of the Kohn-Sham electronic structure of DFT with or without crystal local field effects (LFEs) [14,17], or the *GW* approximation [18], which both neglect excitonic effects. The proposal for direct detection of DM using scintillating materials [19] such as GaAs and NaI has gained relevance since cryogenic scintillating calorimeters have recently reached the required sensitivity and the detection scheme is advantageous for background discrimination [20]. The detection signal consists of photons arising from electron-hole recombination following excitation by a DM particle (Fig. 1). In this mechanism, the attractive interaction between the excited conduction band (CB) electron and the remaining valence band (VB) hole, which form an electron-hole bound state called exciton, will likely affect the scattering rate. For example, an increase in the density of states near the CB edge owing to exciton formation might increase the differential DM-electron scattering rate at low deposited energy, particularly for large band gap scintillators such as NaI. Notably, the typical momentum transfer in the nonrelativistic scattering of a DM particle with a bound electron is $\mathcal{O}(1)$ keV [19] $\simeq \text{\AA}^{-1}$, far from the optical limit $k \rightarrow 0$ studied (with rare exceptions [21–23]) in the context of excitons in solid-state physics. To date, these excitonic effects have not been examined in the DM literature. Since

*Contact author: nora.taufertshoefer@mat.ethz.ch

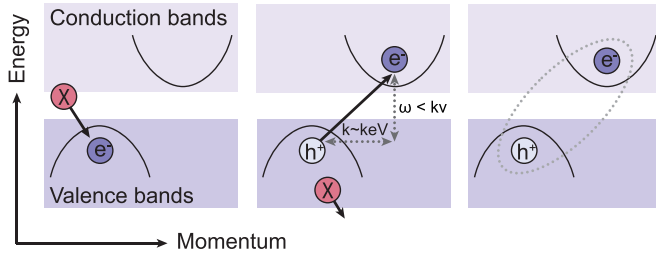


FIG. 1. Schematic of finite-momentum exciton creation by DM-electron scattering in solid-state targets.

NaI and GaAs are the detector materials used by experiments that are specifically designed to measure scintillation signals (NaI in COSINUS [24,25]; GaAs in TESSERACT [26] and DAREDEVIL [27]), determining the impact of electron-hole interactions in these materials is necessary for reliable theoretical support.

Motivated by these considerations, here we solve the Bethe-Salpeter equation (BSE) [28–31] to calculate the frequency- and momentum-dependent dielectric function of GaAs and NaI within *ab initio* MBPT and describe their target response in DM-electron scattering events. With respect to previous works limited to the RPA level, the BSE inherently captures electron-hole interaction excitonic effects. By comparing our BSE and RPA calculations, we are able to quantify the impact of finite-momentum excitonic effects on direct DM searches with NaI and GaAs targets. Our main finding is that for both materials, the BSE approach predicts a larger ELF at low energies compared to that of RPA across a large finite-momentum range, and that the effect is much more pronounced in NaI. This property of the BSE ELF increases the DM-electron scattering rate at energies on the order of the band gap. The increase in the BSE rate in turn leads to an almost one order of magnitude higher predicted cross-section sensitivity in NaI for DM particles with a mass larger than 2 MeV and including a realistic background rate. Our findings suggest that for large band gap scintillators, the inclusion of excitonic effects is essential for predicting the DM-electron scattering rate at low energy and the cross-section sensitivity over the light DM mass range. Conversely, from a condensed matter point of view, scattering with DM will allow excitation of finite-momentum excitons that are unavailable (dark) to optical absorption and, for the highest momenta, outside the range of x-ray scattering spectroscopy.

This paper proceeds as follows: First, for the benefit of the condensed-matter community, we summarize the formalism for calculating the DM-electron scattering rate in terms of the dielectric function, following Ref. [14]. Second, for the benefit of the DM community, we briefly introduce the MBPT formalism and the approaches used to calculate the dielectric function, namely, BSE and RPA with or without LFE. Next, we show our results for the ELF and the differential scattering rates calculated with both methods for the two target materials NaI and GaAs. Finally, we present the predicted DM-electron scattering cross-section sensitivity over the mass range of light DM and discuss the implications of our results for the prospects of a dedicated experiment.

II. FORMALISM

A. The DM-electron scattering rate from the dielectric function

As stated above, for the case of nonrelativistic DM, χ , coupling to the electron density in a target material, the DM-electron scattering rate can be formulated in terms of the longitudinal frequency- and momentum-dependent dielectric function $\epsilon(\omega, \mathbf{k})$ [14,15]. [33] An additional field ϕ , which can be a massive or massless, scalar or vector boson, e.g., a dark photon, mediates the (weak) coupling between the standard-model electron and the DM χ . The rate is then given by [14]

$$R = \frac{1}{\rho_T} \frac{\rho_\chi}{m_\chi} \frac{\pi}{\alpha_{\text{em}}} \frac{\bar{\sigma}_e}{\mu_{\chi e}^2} \int d^3v f_\chi(v) \times \int \frac{d^3k}{(2\pi)^3} k^2 |F_\phi(k)|^2 \times \int \frac{d\omega}{2\pi} \frac{1}{1 - e^{-\beta\omega}} \text{Im} \left[\frac{-1}{\epsilon(\omega, \mathbf{k})} \right] \delta \left(\omega + \frac{k^2}{2m_\chi} - \mathbf{k} \cdot \mathbf{v} \right), \quad (1)$$

where ρ_T is the target density, $\rho_\chi = 0.4 \text{ GeV/cm}^3$ is the local DM density, m_χ is the variable DM mass, α_{em} is the fine structure constant, β is the inverse temperature, $\mu_{\chi e}$ is the reduced mass for DM and electron, and $\bar{\sigma}_e$ is a reference cross section defined in the Supplemental Material [32]. In this work, we consider two limiting cases for the DM-mediator form factor, namely, $F_\phi(k) = \alpha_{\text{em}}^2 m_e^2 / k^2$ for a massless mediator where m_e is the electron mass and $F_\phi(k) = 1$ for a massive mediator. The rate includes an integration over the DM velocity distribution $f_\chi(v)$, which is assumed to follow the standard halo model with details given in the Supplemental Material [32]. Finally, the term in Eq. (1) containing the inverse dielectric function $-\text{Im}\epsilon^{-1}(\omega, \mathbf{k})$ is precisely the ELF, which captures the rate at which an electron loses energy and momentum when traversing a target dielectric material. We emphasize again that this formulation for the DM-electron scattering rate distills the electronic part of the problem into one quantity, the dielectric function $\epsilon(\omega, \mathbf{k})$, which can be calculated using condensed-matter *ab initio* theories. The level of theory can then be selected depending on which physical effects, such as in-medium screening, or single-particle or collective excitations are important for determining the DM-electron rate. The relevant energy and momentum range can also be selected, noting that the Dirac delta in Eq. (1) ensures the kinematic relation for the energy deposition as a function of the transferred momentum \mathbf{k} , $\omega = \mathbf{k} \cdot \mathbf{v} - k^2/(2m_\chi)$ [6]. Hence, the energy deposited in a DM-electron scattering event is constrained by $\omega < kv$. Within the employed standard halo model, the DM velocity is bounded by $v \lesssim v_{\text{esc}} + v_{\text{Earth}}$ [19]. For example, using $v = 740 \text{ km/s}$, a transferred momentum of $k = 10 \text{ keV}$ can result from energy depositions $\omega_{k=10 \text{ keV}} \leq 25 \text{ eV}$. This energy range, in which excitonic effects are typically important in semiconducting systems, further justifies our choice of the BSE to calculate the ELF.

B. The dielectric function from BSE and RPA

In a compact form, the BSE can be written as [30]

$$L = L^0 + L^0 \Xi L, \quad (2)$$

where $L(x_1, x_2; x_3, x_4)$ is the two-particle correlation function [with $x_i = (t_i, \mathbf{r}_i)$ the space-time four-vector], $L^0(x_1, x_2; x_3, x_4) = G(x_2, x_4)G(x_3, x_1)$ with G the one-particle Green's function, and the BSE kernel $\Xi = \delta\Sigma/\delta G$ defined as the functional derivative of the irreducible self-energy Σ with respect to G . In the GW approximation for the mass operator, $\Sigma_M = iGW$, the kernel becomes $\Xi(x_1, x_2; x_3, x_4) = -i\delta(x_1, x_2)\delta(x_3, x_4)\delta(t_1, t_3)v(\mathbf{r}_1, \mathbf{r}_3) + i\delta(x_1, x_3)\delta(x_2, x_4)\delta(t_1, t_2)W(\mathbf{r}_2, \mathbf{r}_1, \omega = 0)$ in terms of the bare Coulomb interaction v and the statically ($\omega = 0$) screened electron-hole attraction W . In the standard approach employed in this work, the screening W^{RPA} is derived from a separate RPA calculation. Here, we solve the BSE within the Tamm-Dancoff approximation (TDA), which neglects the coupling between the resonant and the antiresonant parts; i.e., it neglects electron-hole pairs propagating backward in time. Once the BSE is solved for L , we calculate the polarizability $\chi(x_1, x_2) = -iL(x_1, x_2; x_1^+, x_2^+)$ [where $x_i^+ = (t_i + 0^+, \mathbf{r}_i)$], and the inverse microscopic dielectric function $\varepsilon^{-1} = 1 + v\chi$. The Fourier transform then provides the macroscopic dielectric function including LFE $\varepsilon_M(\mathbf{k} = \mathbf{q} + \mathbf{G}, \omega) = 1/\varepsilon_{\mathbf{G}\mathbf{G}}^{-1}(\mathbf{q}, \omega)$ (with \mathbf{q} within the first Brillouin zone and \mathbf{G} a reciprocal lattice vector), which enters Eq. (1). We compare the BSE results capturing excitonic effects to RPA, which is retrieved by neglecting the electron-hole screened interaction W in the kernel Ξ of Eq. (2). Excluding crystal LFE in RPA (or in BSE) neglects microscopic contributions of the induced field to the macroscopic response, so that an independent (quasi)particle picture is retrieved.

C. Numerical details on the *ab-initio* calculations

To perform the electronic structure calculations, we use the full-potential all-electron code `exciting` [34,35], which allows us to avoid the difficulties associated with the widely

used pseudopotential approximation [9] and to directly capture the high-momentum components of the valence and semicore states. First, we carry out ground-state DFT calculations within the local density approximation for both GaAs and NaI, with details given in the Supplemental Material [32]. We then apply quasiparticle corrections to the DFT Kohn-Sham electronic structure. For coherence with the BSE kernel, this is usually done by a GW self-energy. Here, for the sake of comparison with the previous literature, we used a scissor operator matched to reproduce the experimental band gaps $E_g^{\text{GaAs}} = 1.519$ eV [36] and $E_g^{\text{NaI}} = 5.9$ eV [37]. The resulting band structures are shown in the Supplemental Material [32].

For a valid comparison of the ELF from RPA and BSE, we use the same underlying scissor-corrected Kohn-Sham states as a starting point for both methods. As the BSE approach is computationally expensive, scaling to the third power of the number of k -points and included bands, we opted for a balanced setup in terms of VBs, CBs, and k -grid resolution. A $6 \times 6 \times 6$ k -grid and up to 14 bands in total offer a good compromise between accuracy and cost. For GaAs (NaI), selecting four VBs (three VBs) and ten CBs allows us to capture all electron-hole excitations in an energy range spanned by the highest VB and CB up to ~ 12 eV. We then use the same computational parameters tested for BSE in RPA, with the exception that we include the semicore states that, however, do not contribute in the low-energy range of interest. In the Supplemental Material [32], we briefly discuss excitonic effects for the Ga $3d$ semicore states when a larger energy range is considered.

III. RESULTS

A. Energy loss functions and DM-electron scattering rates

For deriving the DM-electron scattering rates, we use the open-source code `DarkELF` [17,38] with our computed ELFs

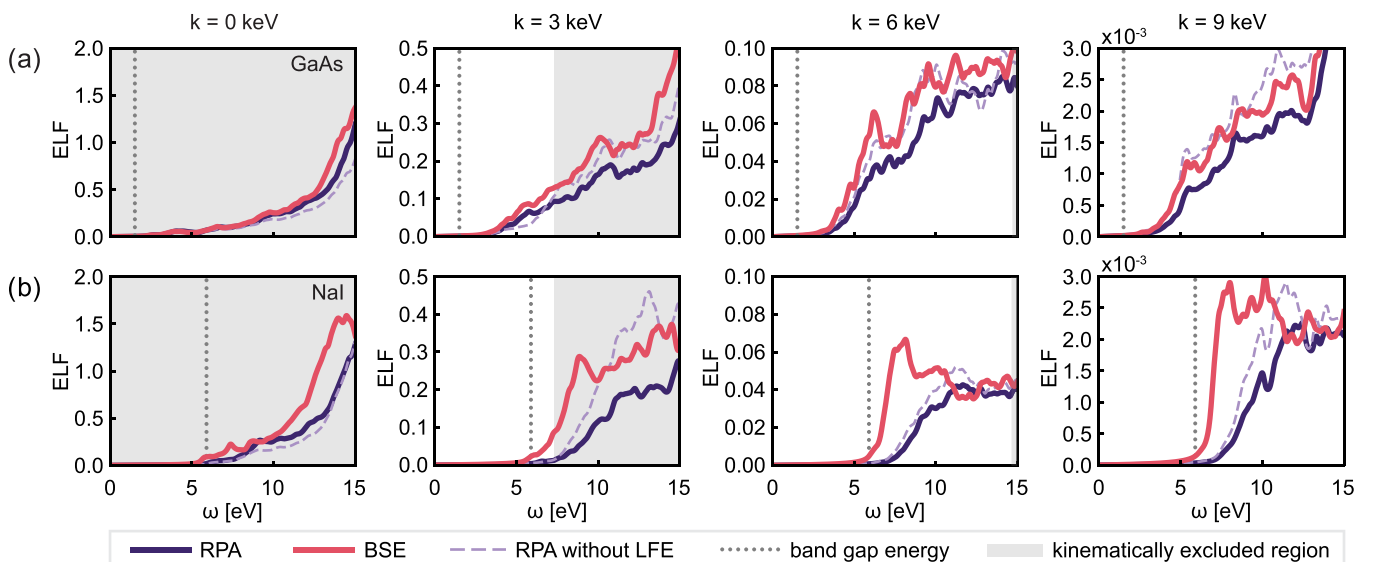


FIG. 2. ELF at various transferred momenta calculated with RPA and BSE for (a) GaAs and (b) NaI. At low energies, the ELF from BSE is always larger than that from RPA due to the excitonic contributions, with the largest difference for NaI. The ELF for RPA without LFE corresponds to independent particle transitions. Gray shaded regions indicate the kinematically excluded energy range for DM-electron scattering, assuming the maximum DM speed is 740 km/s.

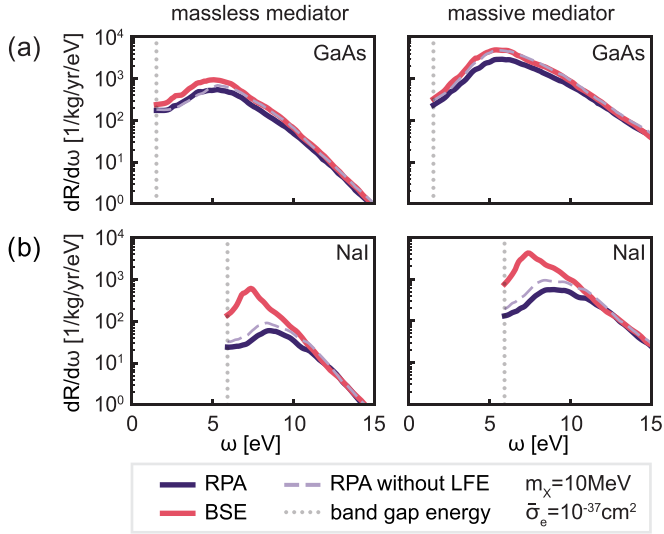


FIG. 3. Differential scattering rates for (a) GaAs and (b) NaI calculated with RPA and BSE for the limiting cases of a massless and a massive mediator. The underlying dielectric functions include ten CBs and transferred momenta $|\mathbf{k}| = [0, 0.3, 0.7, 1.0, \dots, 14.7]$ keV.

and restrict our study to isotropic responses, in which the dielectric function depends only on the absolute value of the momentum $|\mathbf{k}|$. We now compare our ELF calculations within RPA and BSE for the two materials GaAs and NaI, using ten CBs in each case for consistency. Figure 2 shows the ELF in the low-energy range up to $\omega = 15$ eV in the optical limit ($k = 0$) and at three nonzero values of momentum transfer ($k = 3, 6,$ and 9 keV). For both materials, the BSE ELF is larger than the RPA ELF in this energy range due to the excitonic contributions. The BSE increase is strong for NaI, particularly at energies near the band gap, while in GaAs it is smaller and of similar size over the displayed energy range. For NaI, the lowest excitonic contributions to the ELF below the band gap energy are subtle but visible for $k = 0$ and $k = 3$ keV. Excluding LFE in RPA leads to an increased ELF at finite momentum that even partially exceeds the BSE ELF at larger energies. For technical details, we refer to the Supplemental Material [32].

The properties of the ELF in the kinematically allowed region (see Fig. 2) are directly transferred to the scattering rates, which we present next. Figure 3 shows the differential scattering rates for the massless and massive mediator case, including transferred momenta up to 14.7 keV. The DM mass and reference cross section are fixed to $m_\chi = 10$ MeV and $\bar{\sigma}_e = 1 \times 10^{-37}$ cm², respectively.

For GaAs, the BSE rate is only slightly larger at low energies compared to that of RPA, and the overall shape is similar as expected from Fig. 2(a). In contrast, for NaI, we observe a significantly larger BSE rate, which peaks at about 8 eV. This feature is due to the large contributions of the ELF at higher momentum transfers, as shown in Fig. 2(b). Excluding LFE in RPA slightly increases the rate since local screening effects are neglected. For GaAs and a massive mediator, the BSE rate and that for RPA without LFE even overlap due to the similar ELF at finite momentum.

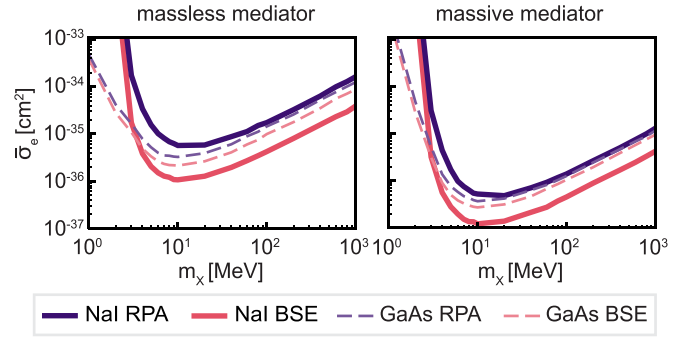


FIG. 4. Reach over the light dark matter range for GaAs and NaI for a kg-year exposure, assuming a monotonically decaying background. The BSE approach predicts a better sensitivity, in particular, for NaI.

B. Cross-section sensitivity including an experimental background

Next, we present the cross-section sensitivity for GaAs and NaI based on our rate calculations using BSE and RPA over the light DM mass range. For a kg-year exposure, we assume a monotonically decaying experimental background in the light detector [39] with the number of events of the order 10^9 , including a suppression factor of $\lambda_{\text{bck}} = 10^{-4}$, following the method in Ref. [20]. Further details are given in the Supplemental Material [32]. For NaI, we assume an absorption onset at 5.6 eV, corresponding to the lowest energy exciton absorption peak in optical measurements [40], and 4.2 eV for emission, corresponding to electron-hole recombination from the self-trapped exciton [41]. For GaAs, we use the measured band gap value of 1.519 eV [36] for absorption, justified by the small binding energy of ~ 3 meV of the lowest optical exciton [42], and the reported value 1.48 eV for emission [43]. We consider a combined light yield and collection efficiency of $\epsilon_l = 13\%$ according to Ref. [44] for NaI and choose the same value for GaAs for comparison. Note that doped GaAs can achieve light yields that are significantly higher than those of pure crystals [43]. We plot the resulting reach for both massless and massive mediators over a range of light DM masses in Fig. 4, and see that the BSE method yields a better sensitivity than the RPA for the full mass range. While this improvement is moderate for GaAs, excitonic effects in NaI improve the reach by almost an order of magnitude. The smallest considered DM mass cannot be probed with NaI as the low-energy threshold in the scattering rate is still almost 4 times larger than that in GaAs, even when accounting for the lowest exciton.

IV. SUMMARY AND CONCLUSION

In this work, we showed that excitonic effects captured in the BSE ELF increase the predicted DM-electron scattering rate at low energy compared with predictions from the RPA method. This effect is considerably more pronounced for NaI, which has an exciton binding energy that is 2 orders of magnitude larger than that of GaAs in the optical limit [45,46]. Therefore, our results suggest that electron-hole interactions in scattering events with finite-momentum transfer

have a greater impact in materials with stronger bound optical excitons. Importantly, we found that excitonic effects are significant even at large momentum transfer, where intuition from optical experiments is limited. The discovery of an increased BSE DM-electron scattering rate allowed us to report improved cross-section sensitivities for both GaAs and NaI detectors considering a realistic background rate. The substantial improvement of the reach for NaI highlights that accounting for excitonic effects is necessary for accurately describing the response in this target material. We note that neither coupling to antiresonant electron-hole transitions beyond the TDA at finite-momentum transfer nor correlation effects beyond the *GW* approximation to the BSE adiabatic-only kernel Ξ are included in our calculations, opening a perspective for future theoretical developments. Likewise, nonradiative relaxation processes that lead to the formation of self-trapped excitons in NaI [41,47] and the energy dependence of the emission are not studied here. While self-trapping of excitons could in principle be captured in first-principles calculations [48], both processes might be more effectively incorporated through phenomenological modeling based on experimental measurements. Indeed, the measurement of electronic excitations in cryogenic scintillating calorimeters is the scope of a dedicated detector and phenomenology development—the OvDES project—in collaboration with the COSINUS experiment [20,25]. Our work

emphasizes the importance of such accurate calibration of the cryogenic scintillating calorimeters for DM-electron scattering searches, as well as the desirability of calibration sources inducing finite-momentum excitons over light sources.

ACKNOWLEDGMENTS

We thank Tanner Trickle, Karoline Schäffner, and Paolo Settembri for helpful discussions. N.T., R.C., and N.A.S. acknowledge support from the Swiss National Science Foundation under Grant No. 10002603. N.A.S. and V.O. thank the CNRS Fellow Ambassador program for supporting N.A.S.’s visit to the Institut Néel. V.Z. acknowledges the support of the Klaus Tschira Foundation to the OvDES project. R.C. acknowledges support from an individual research grant from the Swedish Research Council (Dnr. 2022-04299) and from the “Light Dark Matter” project (Dnr. KAW 2019.0080) funded by the Knut and Alice Wallenberg Foundation. Computational resources were provided by the ETH Zurich Euler cluster.

DATA AVAILABILITY

The relevant input files of our *ab initio* calculations and the data supporting the findings of this work are publicly available [49].

-
- [1] J. Billard, M. Boulay, S. Cebrián, L. Covi, G. Fiorillo, A. Green, J. Kopp, B. Majorovits, K. Palladino, F. Petricca, L. Roszkowski, and M. Schumann, Direct detection of dark matter—APPEC committee report, *Rep. Prog. Phys.* **85**, 056201 (2022).
 - [2] R. Essig, Some progress & challenges for the direct-detection of sub-GeV dark matter, *Nucl. Phys. B* **1003**, 116484 (2024).
 - [3] J. Kopp, V. Niro, T. Schwetz, and J. Zupan, DAMA/LIBRA data and leptonically interacting dark matter, *Phys. Rev. D* **80**, 083502 (2009).
 - [4] A. Dedes, I. Giomataris, K. Suxho, and J. Vergados, Searching for secluded dark matter via direct detection of recoiling nuclei as well as low energy electrons, *Nucl. Phys. B* **826**, 148 (2010).
 - [5] R. Essig, J. Mardon, and T. Volansky, Direct detection of sub-GeV dark matter, *Phys. Rev. D* **85**, 076007 (2012).
 - [6] R. Essig, M. Fernández-Serra, J. Mardon, A. Soto, T. Volansky, and T.-T. Yu, Direct detection of sub-GeV dark matter with semiconductor targets, *J. High Energy Phys.* **05** (2016) 046.
 - [7] S. M. Griffin, K. Inzani, T. Trickle, Z. Zhang, and K. M. Zurek, Multichannel direct detection of light dark matter: Target comparison, *Phys. Rev. D* **101**, 055004 (2020).
 - [8] S. M. Griffin, Y. Hochberg, K. Inzani, N. Kurinsky, T. Lin, and T. C. Yu, Silicon carbide detectors for sub-GeV dark matter, *Phys. Rev. D* **103**, 075002 (2021).
 - [9] S. M. Griffin, K. Inzani, T. Trickle, Z. Zhang, and K. M. Zurek, Extended calculation of dark matter-electron scattering in crystal targets, *Phys. Rev. D* **104**, 095015 (2021).
 - [10] H.-Y. Chen, A. Mitridate, T. Trickle, Z. Zhang, M. Bernardi, and K. M. Zurek, Dark matter direct detection in materials with spin-orbit coupling, *Phys. Rev. D* **106**, 015024 (2022).
 - [11] C. E. Dreyer, R. Essig, M. Fernandez-Serra, A. Singal, and C. Zhen, Fully *ab-initio* all-electron calculation of dark matter-electron scattering in crystals with evaluation of systematic uncertainties, *Phys. Rev. D* **109**, 115008 (2024).
 - [12] R. Catena, T. Emken, N. A. Spaldin, and W. Tarantino, Atomic responses to general dark matter-electron interactions, *Phys. Rev. Res.* **2**, 033195 (2020).
 - [13] R. Catena, T. Emken, M. Matas, N. A. Spaldin, and E. Urdshals, Crystal responses to general dark matter-electron interactions, *Phys. Rev. Res.* **3**, 033149 (2021).
 - [14] S. Knapen, J. Kozaczuk, and T. Lin, Dark matter-electron scattering in dielectrics, *Phys. Rev. D* **104**, 015031 (2021).
 - [15] Y. Hochberg, Y. Kahn, N. Kurinsky, B. V. Lehmann, T. C. Yu, and K. K. Berggren, Determining dark-matter–electron scattering rates from the dielectric function, *Phys. Rev. Lett.* **127**, 151802 (2021).
 - [16] J. Lindhard, On the properties of a gas of charged particles, *Kgl. Danske Videnskab. Selskab, Mat. Fys. Medd.* **28**, 21 (1954).
 - [17] S. Knapen, J. Kozaczuk, and T. Lin, Python package for dark matter scattering in dielectric targets, *Phys. Rev. D* **105**, 015014 (2022).
 - [18] E. A. Peterson, S. L. Watkins, C. Lane, and J.-X. Zhu, Beyond-DFT *ab initio* calculations for accurate prediction of sub-GeV dark matter experimental reach, [arXiv:2310.00147](https://arxiv.org/abs/2310.00147).
 - [19] S. Derenzo, R. Essig, A. Massari, A. Soto, and T.-T. Yu, Direct detection of sub-GeV dark matter with scintillating targets, *Phys. Rev. D* **96**, 016026 (2017).

- [20] V. Zema, P. Figueroa, G. Angloher, M. R. Bharadwaj, T. Frank, M. N. Hughes, M. Kellermann, F. Pröbst, K. Schäffner, K. Shera, and M. Stahlberg, Dark matter-electron scattering search using cryogenic light detectors, *Phys. Rev. D* **110**, 123012 (2024).
- [21] M. Gatti and F. Sottile, Exciton dispersion from first principles, *Phys. Rev. B* **88**, 155113 (2013).
- [22] H.-C. Weissker, J. Serrano, S. Huotari, E. Luppi, M. Cazzaniga, F. Bruneval, F. Sottile, G. Monaco, V. Olevano, and L. Reining, Dynamic structure factor and dielectric function of silicon for finite momentum transfer: Inelastic x-ray scattering experiments and *ab initio* calculations, *Phys. Rev. B* **81**, 085104 (2010).
- [23] P. Abbamonte, T. Graber, J. P. Reed, S. Smadici, C.-L. Yeh, A. Shukla, J.-P. Rueff, and W. Ku, Dynamical reconstruction of the exciton in LiF with inelastic x-ray scattering, *Proc. Natl. Acad. Sci. USA* **105**, 12159 (2008).
- [24] G. Angloher, M. R. Bharadwaj, I. Dafinei, N. Di Marco, L. Einfalt, F. Ferroni, S. Fichtinger, A. Filipponi, T. Frank, M. Friedl, A. Fuss, Z. Ge, M. Heikinheimo, M. N. Hughes, K. Huitu, M. Kellermann, R. Maji, M. Mancuso, L. Pagnanini, and F. Petricca (COSINUS Collaboration), Deep-underground dark matter search with a COSINUS detector prototype, *Phys. Rev. D* **110**, 043010 (2024).
- [25] G. Angloher, M. R. Bharadwaj, A. Böhmer, M. Cababie, I. Colantoni, I. Dafinei, N. D. Marco, C. Dittmar, L. Einfalt, F. Ferella, *et al.*, COSINUS—A model-independent challenge of the DAMA/LIBRA dark matter claim with cryogenic NaI detectors operated in a new low-background facility, [arXiv:2507.02429](https://arxiv.org/abs/2507.02429).
- [26] R. Essig, G. K. Giovanetti, N. Kurinsky, D. McKinsey, K. Ramanathan, K. Stifter, T.-T. Yu, A. Aboubrahim, D. Adams, D. S. M. Alves, *et al.*, Snowmass2021 Cosmic Frontier: The landscape of low-threshold dark matter direct detection in the next decade, [arXiv:2203.08297](https://arxiv.org/abs/2203.08297).
- [27] D. L. Helis, A. Melchiorre, A. Puiu, G. Benato, P. Carniti, A. Continenza, N. Di Marco, A. Ferella, C. Ferrari, F. Giannessi, *et al.*, First measurement of gallium arsenide as a low-temperature calorimeter, *Eur. Phys. J. C* **84**, 749 (2024).
- [28] E. E. Salpeter and H. A. Bethe, A relativistic equation for bound-state problems, *Phys. Rev.* **84**, 1232 (1951).
- [29] W. Hanke and L. J. Sham, Many-particle effects in the optical excitations of a semiconductor, *Phys. Rev. Lett.* **43**, 387 (1979).
- [30] G. Strinati, Application of the Green's functions method to the study of the optical properties of semiconductors, *Riv. Nuovo Cimento* **11**, 1 (1988).
- [31] G. Onida, L. Reining, R. W. Godby, R. Del Sole, and W. Andreoni, *Ab initio* calculations of the quasiparticle and absorption spectra of clusters: The sodium tetramer, *Phys. Rev. Lett.* **75**, 818 (1995).
- [32] See Supplemental Material at <http://link.aps.org/supplemental/10.1103/9b1j-fcvw> for additional details on the electronic structure calculations, the dark matter model, and the reach calculations, which includes Refs. [50–53].
- [33] In principle, we can also consider the coupling with the electron current for the case, e.g., of a vector boson mediator. This case requires the calculation of the full dielectric tensor, including transverse components.
- [34] A. Gulans, S. Kontur, C. Meisenbichler, D. Nabok, P. Pavone, S. Rigamonti, S. Sagmeister, U. Werner, and C. Draxl, Exciting: A full-potential all-electron package implementing density-functional theory and many-body perturbation theory, *J. Phys.: Condens. Matter* **26**, 363202 (2014).
- [35] C. Vorwerk, B. Aurich, C. Cocchi, and C. Draxl, Bethe–Salpeter equation for absorption and scattering spectroscopy: Implementation in the exciting code, *Electron. Struct.* **1**, 037001 (2019).
- [36] E. Grilli, M. Guzzi, R. Zamboni, and L. Pavesi, High-precision determination of the temperature dependence of the fundamental energy gap in Gallium arsenide, *Phys. Rev. B* **45**, 1638 (1992).
- [37] F. C. Brown, C. Gähwiller, H. Fujita, A. B. Kunz, W. Scheifley, and N. Carrera, Extreme-ultraviolet spectra of ionic crystals, *Phys. Rev. B* **2**, 2126 (1970).
- [38] B. Campbell-Deem, S. Knapen, J. Kozaczuk, T. Lin, C. Stratman, and E. Villarama, DarkELF Python code, GitHub (2022, <https://github.com/tongylin/DarkELF>).
- [39] G. Angloher, S. Banik, G. Benato, A. Bento, A. Bertolini, R. Breier, C. Bucci, J. Burkhart, L. Canonica, A. D'Addabbo, S. Di Lorenzo, L. Einfalt, A. Erb, F. v. Feilitzsch, N. Ferreira Iachellini, S. Fichtinger, D. Fuchs, A. Fuss, A. Garai, and V. M. Ghete (CRESST Collaboration), Results on sub-GeV dark matter from a 10 eV threshold CRESST-III silicon detector, *Phys. Rev. D* **107**, 122003 (2023).
- [40] K. Teegarden and G. Baldini, Optical absorption spectra of the alkali halides at 10°K, *Phys. Rev.* **155**, 896 (1967).
- [41] R. Williams and K. Song, The self-trapped exciton, *J. Phys. Chem. Solids* **51**, 679 (1990).
- [42] M. D. Sturge, Optical absorption of Gallium arsenide between 0.6 and 2.75 eV, *Phys. Rev.* **127**, 768 (1962).
- [43] S. Vasiukov, F. Chioffi, C. Braggio, G. Carugno, F. Moretti, E. Bourret, and S. Derenzo, GaAs as a bright cryogenic scintillator for the detection of low-energy electron recoils from MeV/c² dark matter, *IEEE Trans. Nucl. Sci.* **66**, 2333 (2019).
- [44] F. Reindl, G. Angloher, P. Carniti, L. Cassina, L. Gironi, C. Gotti, A. Gütlein, M. Maino, M. Mancuso, N. D. Marco, L. Pagnanini, G. Pessina, F. Petricca, S. Pirro, F. Pröbst, R. Puig, K. Schäffner, and J. Schieck, Results of the first NaI scintillating calorimeter prototypes by COSINUS, *J. Phys.: Conf. Ser.* **1342**, 012099 (2020).
- [45] J. E. Eby, K. J. Teegarden, and D. B. Dutton, Ultraviolet absorption of Alkali Halides, *Phys. Rev.* **116**, 1099 (1959).
- [46] M. Grunert, M. Großmann, and E. Runge, Predicting exciton binding energies from ground-state properties, *Phys. Rev. B* **110**, 075204 (2024).
- [47] S. Nagata, K. Fujiwara, and H. Nishimura, Dynamical aspects of excitons in NaI, *J. Lumin.* **47**, 147 (1990).
- [48] Z. Dai, C. Lian, J. Lafuente-Bartolome, and F. Giustino, Excitonic polarons and self-trapped excitons from first-principles exciton-phonon couplings, *Phys. Rev. Lett.* **132**, 036902 (2024).
- [49] N. Taufertshöfer, V. Zema, R. Catena, V. Olevano, and N. A. Spaldin, Replication data and input files for “Excitonic contributions to dark matter-electron scattering” [Data set], Zenodo (2025), <https://doi.org/10.5281/zenodo.17733600>.
- [50] D. Zhou and B. F. Usher, Deviation of the AlGaAs lattice constant from Vegard's law, *J. Phys. D: Appl. Phys.* **34**, 1461 (2001).
- [51] *Handbook of Optics: Design, Fabrication, and Testing; Sources and Detectors; Radiometry and Photometry*, 3rd ed. edited

- by M. Bass (McGraw-Hill Education, New York, 2010), Vol. 2.
- [52] K. Momma and F. Izumi, *Vesta*: A three-dimensional visualization system for electronic and structural analysis, *J. Appl. Crystallogr.* **41**, 653 (2008).
- [53] K. Aggarwal, I. Arnquist, N. Avalos, X. Bertou, N. Castelló-Mor, A. E. Chavarria, J. Cuevas-Zepeda, A. Dastgheibi-Fard, C. D. Dominicis, O. Deligny, *et al.*, Probing benchmark models of hidden-sector dark matter with DAMIC-M, *Phys. Rev. Lett.* **135**, 071002 (2025).